Progress In Electromagnetics Research M, Vol. 114, 219–232, 2022

Cantor-Square Fractal Reconfigurable Circular Patch Antenna with Low Cross-Polarization for X Band Applications

Iqra Masroor*, Shadman Aslam, Jamshed A. Ansari, and Amrees Pandey

Abstract—This work proposes a novel probe-fed circular patch antenna which has been fractaled and reconfigured to deliver enhanced performance. The circular ground plane is made defected using Cantor-square fractal geometry which reduces the cross-polarization level by about 12 dB. Further, by appropriate positioning of a PIN diode switch in the ground slot, the fractal Circular Microstrip Patch Antenna (CMPA) is enabled to achieve frequency reconfiguration. A prototype of the proposed antenna is fabricated and tested for the assessment of various parameters. The proposed fractal reconfigurable antenna has a peak gain well above 6 dB, high radiation efficiency, and a maximum bandwidth of about 700 MHz in the X-band (8–12 GHz). The present work aims to focus on the huge potential of fractal reconfigurable antennas in modern dynamic wireless communication systems.

1. INTRODUCTION

Since their development in the 1970s, microstrip patch antennas continue to govern the vast field of microwave antennas because of their numerous advantages and diversified applications [1]. Low fabrication cost, low volume, ease-of-integration, light weight and thin profile configurations are some of the abundant features that have made them superior to conventional microwave antennas [2]. Their success has led to increasing researches aimed at overcoming the existing limitations such as narrow bandwidth, low gain, high cross-polarization level, and up gradation of the performance parameters. The constant thrust for advancement of microstrip patch antennas has led to novel aspects of fractalization and antenna reconfiguration being implemented in their basic configuration.

Size-reduction to achieve antenna miniaturization, broadband response, and multiband operations can be achieved if fractal geometries are incorporated [3, 4]. The use of Koch-shaped fractal defects on the antenna patch shows a significant antenna size-reduction of about 85% in [5]. Of the many fractal geometries such as Sierpinski, Koch, Hilbert, and Minkowski, Cantor fractals are widely used owing to their simplicity and ease of construction. In [6], a patch slot in the shape of Cantor-square fractal geometry is exploited to obtain dual-band operation. An interesting approach combining Koch and Sierpinski fractals to reduce the patch antenna size by lowering the resonant frequency has been utilized in [7]. In [8], the introduction of a fractal-slot in a notch-loaded patch results in the improvement of return loss and bandwidth, leading to reduction in the side lobe level as well.

The redistribution of antenna properties resulting in reconfiguration allows changing antenna's functionalities and is broadly used nowadays to cope with the rapidly evolving wireless technology under dynamic operating conditions. A reconfigurable antenna can be enabled to achieve frequency reconfiguration, polarization reconfiguration, radiation pattern reconfiguration, or a merge of them known as compound reconfiguration. The reconfiguration property and the technique being used for reconfiguration must be ascertained at the very start of the design process [9]. The insertion of three PIN diode switches in a patch antenna has resulted in obtaining eight 4G LTE frequency bands

Received 30 September 2022, Accepted 5 December 2022, Scheduled 13 December 2022
* Corresponding author: Iqra Masroor (iqraec1029@gmail.com).
The authors are with the Department of Electronics and Communication, University of Allahabad, Prayagraj, India.

in [10]. The loading of RF PIN diode switches on the radiating patch/ground for obtaining frequency reconfigurability has recently been explored in a number of researches [11, 12]. Another technique to achieve frequency reconfigurability by using a variable chip capacitor is presented in [13]. The merge of fractal shapes and reconfiguration in antennas is rapidly gaining the attention of researchers owing to its huge potential applications. This can be observed in [14, 15] wherein fractal Hilbert antennas are proposed exhibiting reconfigurable behavior. Another appealing design of a pattern reconfigurable antenna is described by using dual feed ports [16]. Compound reconfigurability including frequency and radiation pattern reconfiguration can also be achieved by positioning PIN diodes at appropriate places in the slot antenna [17].

Circular microstrip patch antennas are extensively designed because of their simplicity, low manufacturing costs, and conformable structure. In [18], a probe-fed circular patch antenna is proposed for X-band (8–12 GHz) applications. One of the most undesirable features in microstrip antennas is cross polarization which is orthogonal to the desired polarization. Higher cross-polarization is a critical limitation that can often lead to cross-talk in communication systems [19]. A novel aspect to reduce cross polarization using differential feeding in patch antenna array has been presented in [20]. Extensive work has been done to mitigate the problem of high cross-polarization in patch antennas [21, 22]. Fractal Reconfigurable Antennas (FRAs) combine the characteristics of fractal geometries with electronic reconfiguration for providing enhanced antenna performance and can be utilized for multiple and advanced applications [23, 24]. In [25], controlling the capacitance value of a single varactor diode provides about ten different resonating frequencies to a rhombus-shaped fractal microstrip antenna.

Although several FRAs have been proposed in recent literatures, cross-polarization reduction is an important aspect that needs to be dealt with while designing FRAs such that they overcome the existing limitations of patch antennas besides providing enhanced performance. Reconfigurable radiation patterns along with cross-polarization suppression has been achieved in a high gain circular patch antenna by the appropriate loading of slots in [26]. This communication proposes a novel fractal reconfigurable probe-fed circular patch antenna targeted for X-band applications that aims to reduce the cross-polarization level as well. In Section 2, the development and design of the proposed antenna is discussed, followed by Section 3 presenting the simulated and measured results as well as a comparative analysis of the proposed work with previous literatures. In Section 4, the resulting conclusion is given.

2. PROPOSED ANTENNA DESIGN

2.1. Antenna Configuration and Theoretical Considerations

The fundamental configuration of MPA consists of a dielectric substrate with a metallic radiating patch as one surface and a ground plane as the other [1]. MPAs can have patches of different shapes such as rectangle, square, circle, and triangle, depending on the design requirements. In this work, a Circular Microstrip Patch Antenna (CMPA) is designed with successive modifications to its basic configuration for performance improvement. The desired frequency band is X-band (8–12 GHz). Therefore, the center frequency (f_r) chosen for the design is 10 GHz. For the dominant TM_{110} mode, the actual radius (R_p) of the patch for substrate thickness, h, and dielectric constant, ε_r, are obtained using [27]:

$$R_p = \frac{f}{\left\{1 + \frac{2h}{\pi\varepsilon_r f}\left[\ln\left(\frac{\pi f}{2h}\right) + 1.7726\right]\right\}^{1/2}} \tag{1}$$

where,

$$f = \frac{(8.791 \times 10^9)}{(f_r\sqrt{\varepsilon_r})} \tag{2}$$

Rogers RT/duroid 5880 is used as the substrate material with relative permittivity: $\varepsilon_r = 2.2$, dielectric loss tangent: $\delta = 0.0009$, and thickness: $h = 1.57$ mm. Using Equations (1) and (2), $R_p = 5.25$ mm. The radius of the ground plane (R_g) is optimized using parametric analysis such that $R_g = 2 \times R_p = 10.5$ mm. A circular ground plane was chosen to make the design compact and exhibit rotational symmetry. A rectangular ground plane intended for the same 10 GHz resonant frequency, with the same substrate thickness (1.57 mm) and dielectric constant (2.2), would have an area about 18 mm

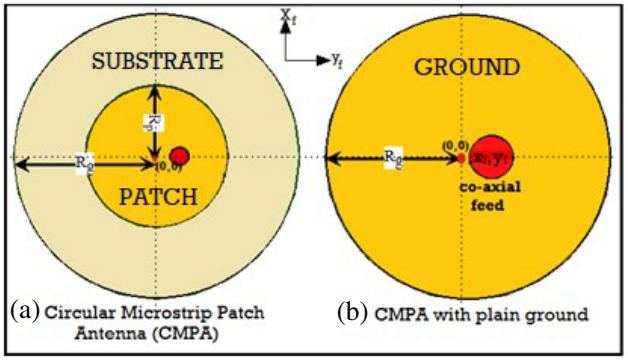

Figure 1. (a) Circular Microstrip Patch Antenna (CMPA), (b) CMPA with plain ground.

$\times$ 21 mm = 378 mm^2 (Length and width of the ground plane can be evaluated using design equations for the rectangular microstrip patch antenna [1]). The proposed circular ground plane, on the other hand, has a reduced area about: $\pi \times R_g^2 = \pi \times 10.5^2 = 346.18\,\text{mm}^2$. Figure 1 illustrates the design schematic of the conventional Circular Microstrip Patch Antenna (CMPA). 50 ohm co-axial probe feed has been utilized to deliver power to the circular metallic patch with the feed-location at (x_f, y_f) to attain proper impedance matching. Probe-feed technique was chosen because one of the principle advantages of this feeding mechanism is that the feed-point can be positioned at any desired location inside the patch so as to achieve impedance matching. Also, the probe-feed technique provides low spurious radiation as compared to other feeding techniques. Determination of the feed-point location and the effect that its displacement causes on the antenna performance is one of the principal requirements while circular patch antennas are designed[18].

2.2. The Cantor-Square Fractal

Mathematician Benoit Mandelbrot coined the term "fractal" in 1975. Fractal geometries are similar patterns at varying scales having properties of self-similarity and space-filling. For fractal geometry, the fractal dimension provides a ratio to depict how the fractal pattern is scaled termed as Hausdorff dimension (H). The Hausdorff dimension is usually an integer for simple shapes, but for less simple fractal geometries, it can have non-integer values as well. One way to calculate it is by using the scaling factor (F) and the number of self-similar shapes (S) in the fractal geometry after the first iteration [28, 29]:

$$H = \frac{\log S}{\log F} \tag{3}$$

A base-motif fractal is the one in which a motif is repeated on a base in every iteration. Cantor square is one such fractal which is constructed as a two-dimensional geometry starting from a square. In every iteration, the square is divided into three horizontal and vertical stripes, in which the middle horizontal and vertical stripes are removed, as shown in Figure 2(a). In this work, the ground plane is fractaled with Cantor square geometry up to two iterations for reducing the cross-polarization level. CMPA with fractal ground is as shown in Figure 2(b). After the first iteration, it can be observed that the scaling factor (F) is 3, and the number of self-similar shapes (S) is 4. Therefore, its Hausdorff dimension is evaluated as:

$$H = \frac{\log S}{\log F} = \frac{\log 4}{\log 3} = 1.2618 \tag{4}$$

2.3. Reconfiguration and Proposed Antenna Design

For obtaining reconfiguration in the fractal ground CMPA, a rectangular slot having dimensions $S_1 \times S_2$ at a distance of 3 mm from x_f and 3.2 mm from y_f is etched on the ground plane. Table 1 depicts

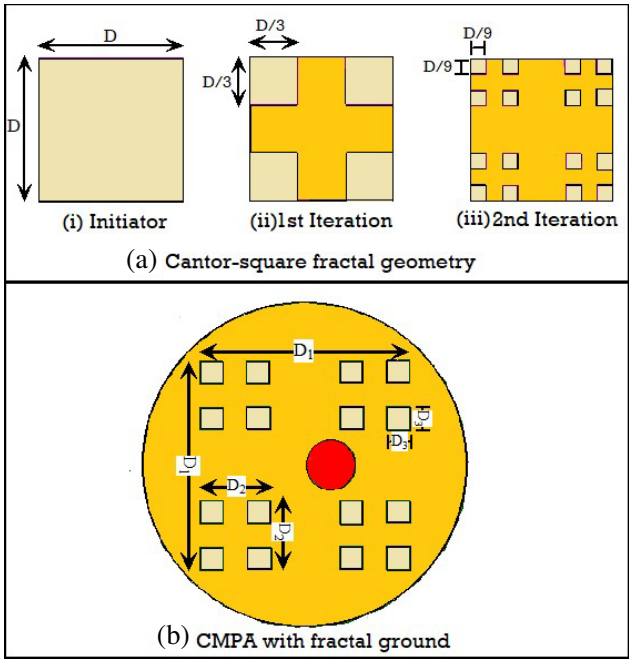

Figure 2. Cantor-square fractal up to 2 iterations, (a) Cantor geometry, (b) CMPA with fractal ground.

Table 1. Dimensions of the proposed antenna.

S. No.	Dimensions	Description	Value (mm)
1.	R_p	Patch radius	5.25
2.	R_g	Ground radius	10.5
3.	D_1	Initiator fractal dimension	13.5
4.	D_2	First iteration fractal dimension ($D_2 = D_1/3$)	4.5
5.	D_3	Second iteration fractal dimension ($D_3 = D_2/3 = D_1/9$)	1.5
6.	S_1	Ground slot length	6
7.	S_2	Ground slot width	1.5
8.	l	Diode length	1.5
9.	w	Diode width	0.9
10.	$(x_f,\ y_f)$	Probe-feed location	(0, 1.7)

the dimensions of the proposed antenna. The final schematic of the proposed CMPA is as shown in Figure 3(a). The top view depicts the circular patch with the feed-point location $(x_f,\ y_f)$, and the bottom-view shows how the PIN diode is positioned in the rectangular slot etched on the circular fractal ground plane.

On the slot etched, a PIN diode, having dimensions $l \times w$, is positioned exactly in the middle of the slot, as shown in Figure 3(b). Using the supply voltage, it is made to switch between forward bias (ON) and reverse bias (OFF) states. In the forward bias state, when the diode is conducting, it is assumed to behave as a series combination of resistance (R_{on}) and inductance (L). In the reverse bias state, when the diode is non-conducting, it is assumed to behave as a parallel combination of resistance (R_{off}) and capacitance (C), with the inductance (L) in series. The PIN diode dimensions used for modeling

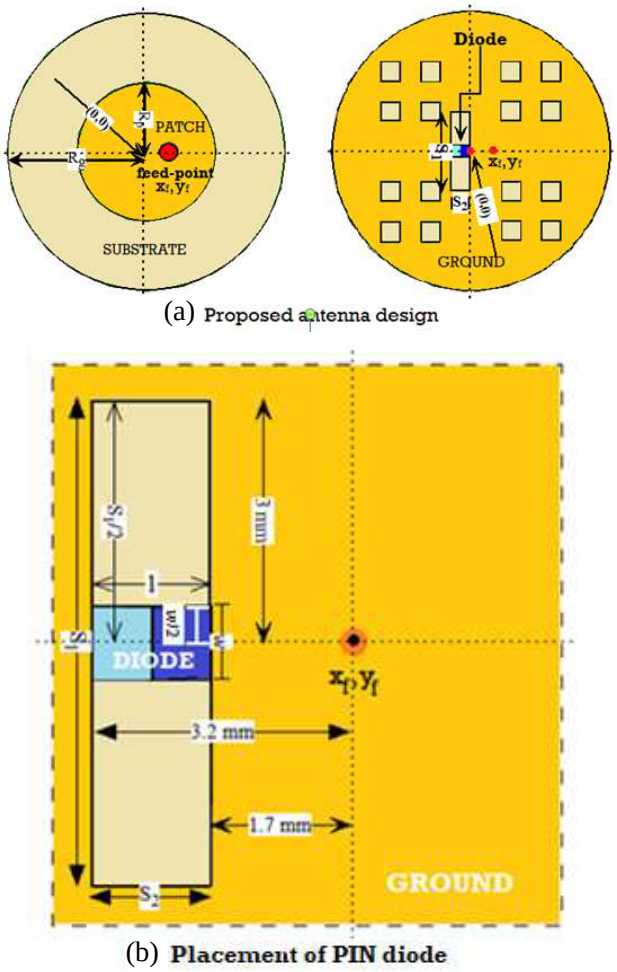

Figure 3. (a) Design of proposed fractal reconfigurable CMPA , (b) placement of PIN diode (zoom-out view of ground plane).

have been obtained from the technical datasheet of Skyworks SMP1340 series, surface-mountable, low-capacitance PIN Diodes [30].

The RLC equivalent circuit of the diode and its HFSS model are as shown in Figure 4. The model values for PIN diode used in the simulation are as depicted in Table 2. The test conditions include a reverse voltage of 50 V which allows a reverse current of 10 µA and a forward voltage of 0.85 V which allows a forward current of 10 mA. This causes the OFF-state resistance to be 0.85 Ω so as to allow current flow through the diode and the ON-state resistance to be 5 MΩ so as to block the flow of current. Typically, the value of L is 0.7 nH, and that of C is 0.21 pF.

Table 2. Model values used for PIN diode simulation.

S. No.	Parameter	Description	Value
1.	L	Series inductance	0.7 nH
2.	R_{on}	ON-state resistance	0.85 Ω
3.	R_{off}	OFF-state resistance	5 MΩ
4.	C	OFF-state capacitance	0.21 pF

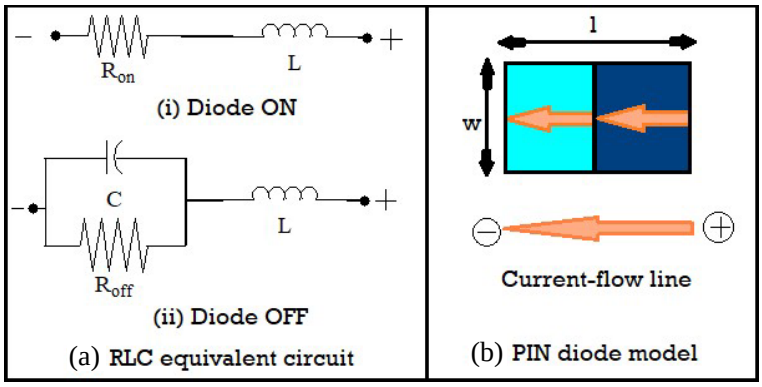

Figure 4. (a) RLC equivalent circuit of PIN diode, (b) PIN diode model.

2.4. Parametric Study

Parametric analysis in terms of the patch radius (R_p) and feed point location (x_f, y_f) is as depicted in Figure 5. It is observed that the resonant frequency decreases with increase in the patch radius (R_p). Decreasing the patch radius below 5.25 mm causes a decrease in the S_{11} parameter. It is observed to be most negative at $R_p = 5.25$ mm, as shown in Figure 5(a). The design is modeled symmetrically on electromagnetic simulation tool HFSS such that the center-point of the circular patch antenna is at coordinates: $(x, y) = (0, 0)$. Keeping the x-coordinate, x_f at 0, the y-coordinate, y_f, has been varied in order to find out the optimum feed-point location where proper impedance matching is obtained. From Figure 5(b), the variation of S_{11} parameter with y_f shows that at $y_f = 1.7$ mm, it is most negative.

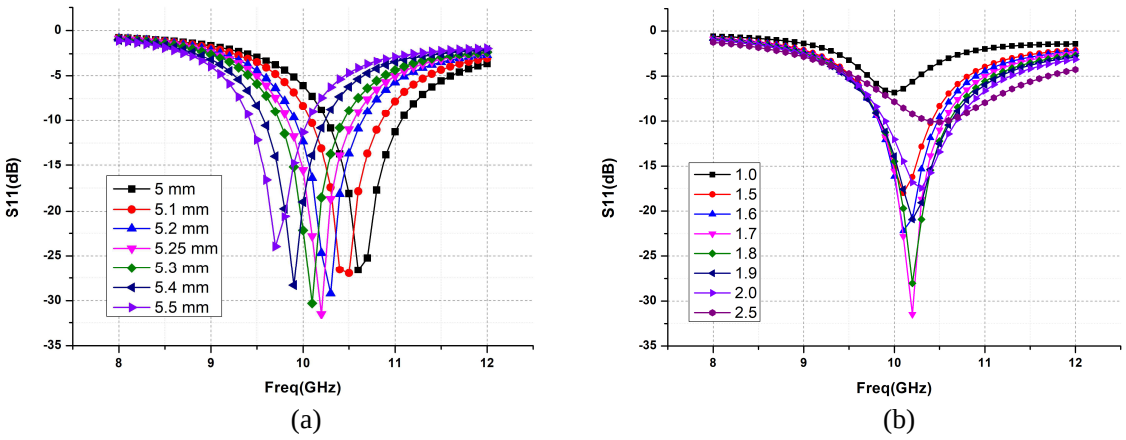

Figure 5. Variation of S_{11} parameter with (a) patch radius (R_P), (b) feed-point (y_f). Variation of S_{11} parameter with Patch radius (R_P). (b) Variation of S_{11} parameter with feed-point (y_f).

3. RESULTS AND DISCUSSION

Finite element method solver Ansys HFSS software has been utilized for modeling and simulation of the proposed antenna. In this section, the simulated and measured results have been investigated, presented, and discussed. A prototype of the proposed antenna has been fabricated and tested using Agilent N5247A: A.09.90.02 Microwave Network Analyzer. For gain and radiation pattern measurements, an anechoic chamber has been used. The distance between the transmitter and receiver is kept to 1.5 m

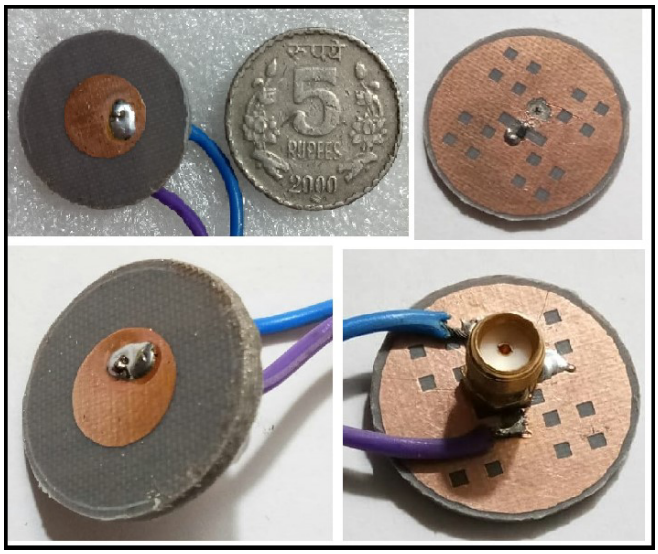

Figure 6. Photographs of the fabricated prototype.

with a transmitted power about $13 \sim 15$ dBm. Photographs of the fabricated prototype, demonstrating the small size and conformable shape of the proposed design, are as shown in Figure 6.

3.1. Cross-Polarization Reduction

The initially designed CMPA having a plain ground is observed to exhibit a cross-polarization of -59.91 dB at the resonant frequency 10.2 GHz. The reflection coefficient at the resonating frequency is about -31.47 dB. After the first fractal iteration, the cross-polarization level is at -59.31 dB. Cantor-dust fractalization on the ground plane up to the second iteration reduces the cross-polarization level by about 12 dB to -72.51 dB, at the same resonant frequency. Henceforth, the impact of making the plain ground fractal is that a considerable reduction in E-plane cross-polarization level is obtained. In the case of plain ground, the cross-polarization level is observed to be about -59.91 dB while in the case of fractaled ground, it is reduced to -72.51 dB. The reflection coefficient, bandwidth, and peak gain at the resonant frequency remain unchanged for plain and fractal grounds, as shown in Figure 7. The

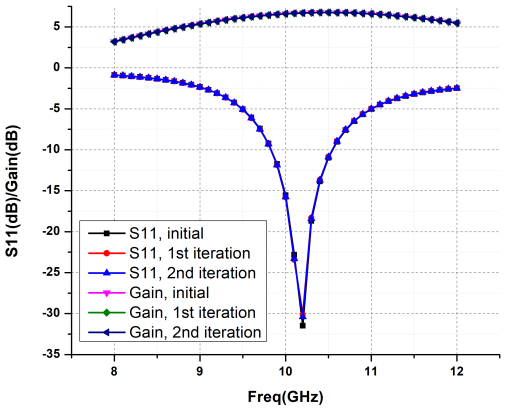

Figure 7. S_{11} and gain of CMPA for plain and fractal grounds.

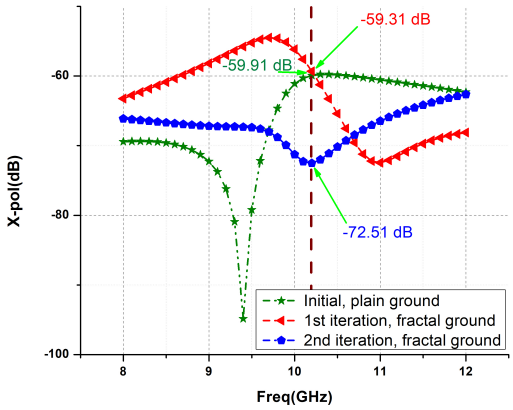

Figure 8. Simulated E-plane cross-polarization levels for plain ground and fractal ground CMPA.

E-plane cross-polarization for the initial plain ground CMPA, first iteration fractal ground CMPA, and second iteration fractal ground CMPA are compared, as illustrated in Figure 8. Further, the addition of reconfiguration using PIN diode to the second iteration fractal ground CMPA has caused the proposed antenna to exhibit frequency switchability in the X band, as discussed under Section 3.2.

3.2. Simulated and Measured Results

Measurement setup of the proposed CMPA using Vector Network Analyzer (VNA) is as demonstrated in Figure 9. The simulated and measured S_{11} parameters of proposed CMPA for ON and OFF diode states are as shown in Figure 10. Two operating bands are obtained in the OFF state of the diode with -10 dB simulated impedance bandwidth of 70 MHz for 9.66 GHz resonant frequency and 600 MHz for 10.22 GHz resonant frequency. A single operating band is obtained in the ON state of the diode with -10 dB simulated impedance bandwidth of 700 MHz for 10.16 GHz resonant frequency. The simulated values obtained for S_{11} parameter, VSWR, and impedance bandwidth of the proposed antenna are as depicted in Table 3.

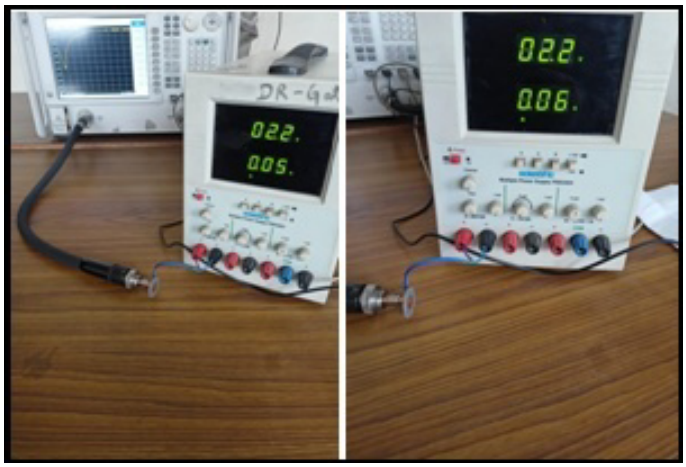

Figure 9. Measurement setup of proposed CMPA with Vector Network Analyzer.

Table 3. Simulated S_{11}, VSWR and impedance bandwidth of proposed CMPA.

Resonant Frequency (GHz)		S_{11} (dB)	VSWR	Impedance Bandwidth (MHz)
Diode OFF	9.66	-13.22	1.55	70 (9.62 GHz–9.69 GHz)
	10.22	-29.49	1.06	600 (9.95 GHz–10.55 GHz)
Diode ON	10.16	-39.59	1.02	700 (9.83 GHz–10.53 GHz)

The gain of proposed CMPA for diode OFF state is observed to be 6.35 dB at 9.66 GHz resonant frequency and 6.70 dB at 10.22 GHz resonant frequency on simulation. For diode ON state, it is observed to be 6.68 dB at 10.16 GHz resonant frequency in simulation. The anechoic chamber setup for measurement of far-field radiation characteristics is as illustrated in Figure 11, and the plot of measured peak gain in dBi as a function of frequency is as illustrated in Figure 12. The lower the cross-polarization level is, the lesser the chances of cross-talk are, and the better the antenna performance is. The cross polarization is significantly reduced in the proposed CMPA. The plot of simulated E-plane cross-polarization level of the proposed CMPA for diode OFF and ON states is as shown in Figure 13. Table 4 depicts the simulated values of gain, cross-polarization level, and radiation efficiency for various diode states. The simulated and measured E-plane and H-plane radiation patterns of the proposed CMPA, for 9.7 GHz and 10.2 GHz, are also illustrated in Figure 14. The radiation patterns

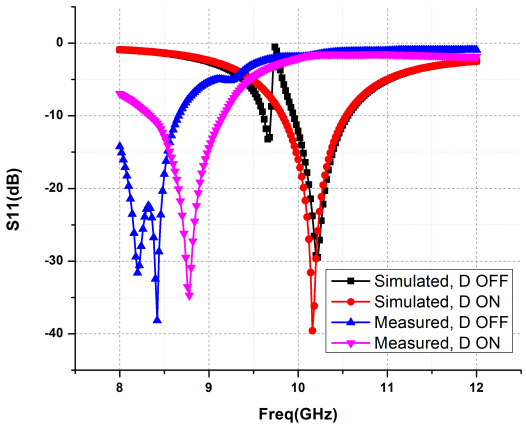

Figure 10. S_{11} of proposed CMPA for diode OFF/ON states.

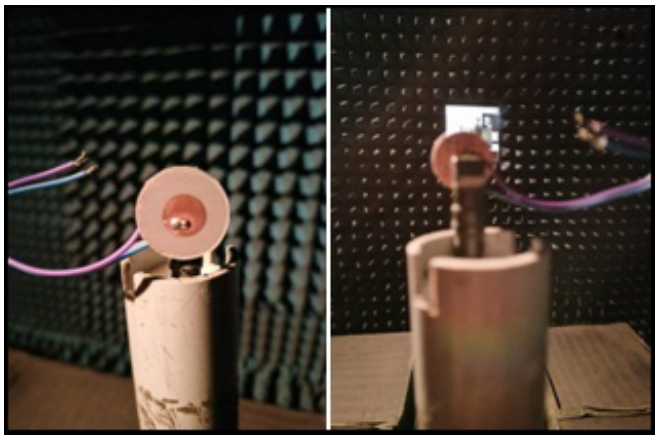

Figure 11. Proposed CMPA in anechoic chamber setup.

are observed to be close to omnidirectional. The reasons for radiation pattern deformation are actually the radiation and reflection losses from the antenna. The proposed CMPA exhibits a high radiation efficiency for both the ON and OFF states of the diode, as illustrated in Figure 15. Discrepancies between simulated and measured results exists due to several factors such as SMA connector, soldering effect, electrical sensitivity of the PIN diode to biasing, and other human errors in fabrication and measurement. Simulated and measured results differ largely due to manufacturing tolerances with respect to the circular cutting of substrate, differences between the ideal and practical behavior of PIN diode, as well as the effect of parasitic elements.

The magnitude of surface current density, J, on the patch is about 21 A/m in the OFF state of

Table 4. Gain, cross-polarization level and radiation efficiency of proposed CMPA.

Resonant Frequency (GHz)		Gain (dB)	Cross polarization (dB)	Radiation efficiency (%)
Diode OFF	9.66	6.35	−63.29	98.95
	10.22	6.70	−85.75	99.23
Diode ON	10.16	6.68	−67.16	99.30

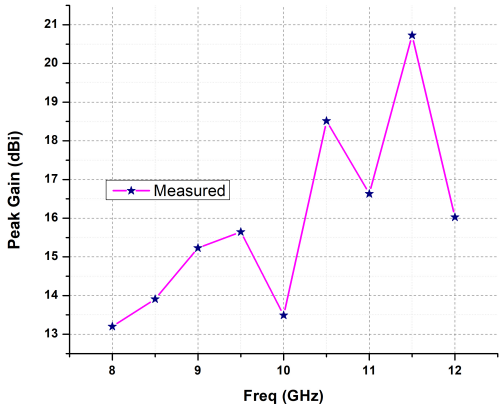

Figure 12. Measured peak gain (dBi) versus frequency plot of proposed CMPA.

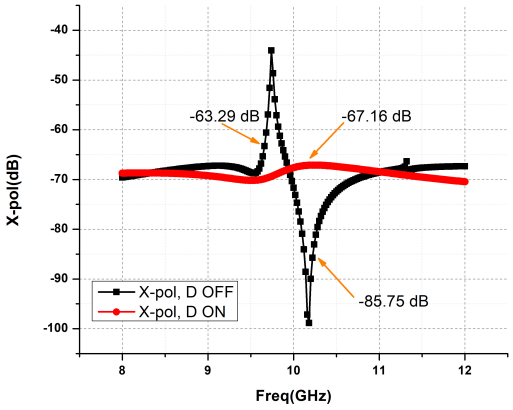

Figure 13. Simulated E-plane cross-polarization level of proposed CMPA for diode OFF and ON states.

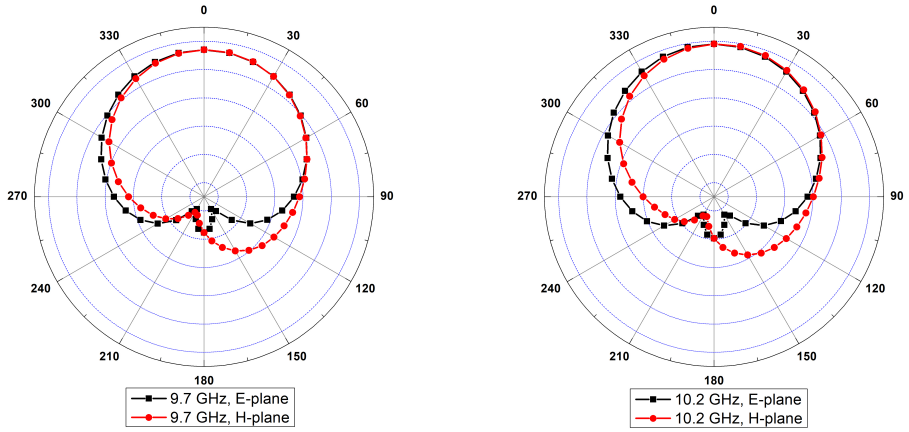

(a) Simulated E and H plane radiation patterns

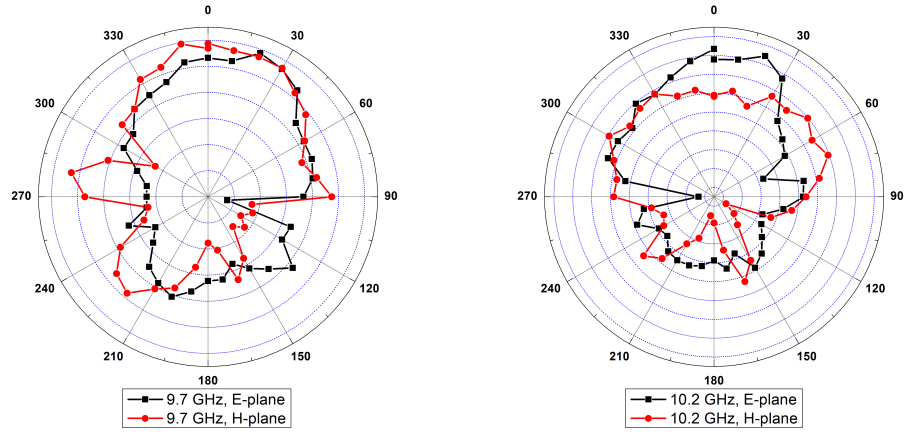

(b) Measured E and H plane radiation patterns

Figure 14. Far-field radiation patterns of the proposed CMPA, (a) simulated E and H plane radiation patterns, (b) measured E and H plane radiation patterns.

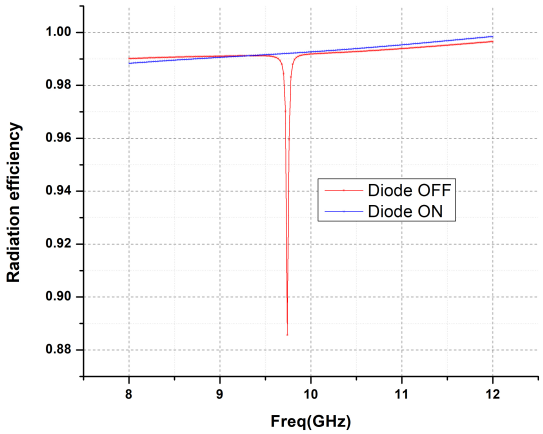

Figure 15. Plot of radiation efficiency of the proposed CMPA for Diode OFF and ON states.

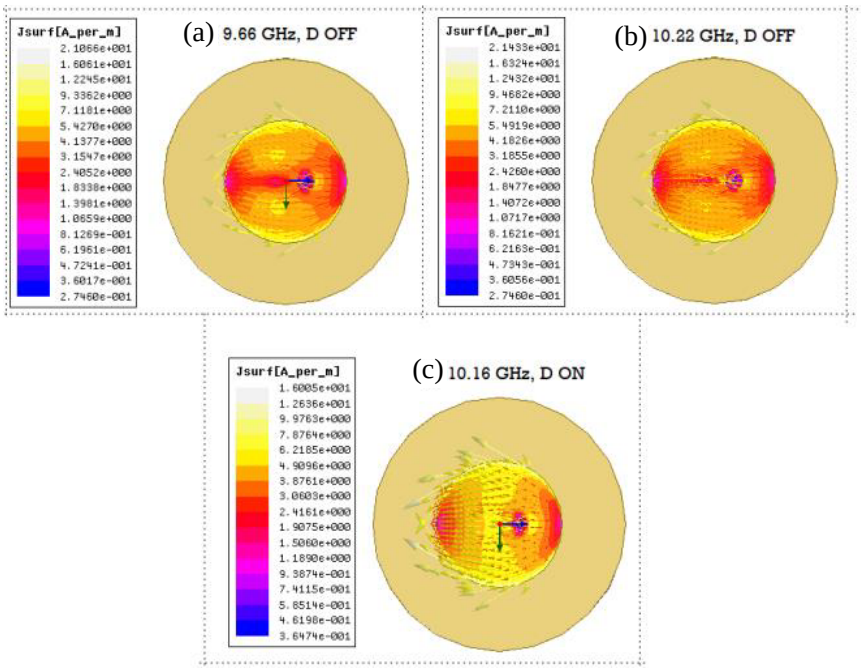

Figure 16. Current density (J) on the patch at (a) 9.66 GHz, D OFF, (b) 10.22 GHz, D OFF and (c) 10.16 GHz, D ON.

the diode and about 16 A/m in the ON state of the diode, as shown in Figure 16. It is observed that the magnitude of current density increases from the centre to the patch periphery along the (vertical) x-axis and decreases from the centre to the patch periphery along the (horizontal) y-axis.

3.3. Comparative Report

A comparative analysis of the proposed work with some existing works [19–22] based on the technique used for cross-polarization reduction is as reported in Table 5. The proposed design not only is reconfigurable but also has a reduced cross polarization level by incorporating a simple technique of fractal ground.

Table 5. Comparative analysis of proposed work with existing works.

References	Technique used for cross-polarization reduction	Cross polarization level (dB)
[19]	Shorted Defected Patch Structure (DPS)	−30
[20]	Differential feed	< -45
[21]	Differential feed	−32
[22]	180 deg Broadband microstrip balun	< -20
Proposed work	Fractal ground	< -63

4. CONCLUSION

In this work, the use of fractalization to obtain cross-polarization reduction has been explored, and the introduction of reconfiguration to the basic antenna configuration has also been presented. The conventional CMPA being transformed to a fractal reconfigurable CMPA has a reduced cross-polarization level and possesses frequency switchability in the X-band. The technique employed for achieving low cross polarization is also simpler than other techniques such as shorted patch, differential feed, or use of microstrip balun. The proposed antenna can be exploited for radar applications, terrestrial and space communications and networking. The intended application at 10 GHz frequency is for X-band radar and satellite communications as well as wireless computer networks. In fact, for terrestrial communications and networking, the X-band 10.15 to 10.7 GHz segment is also utilized in many countries. This communication aims to emphasize the significance of fractalization and reconfiguration in microstrip patch antenna to cater to the needs of dynamic wireless systems and its huge potential for current and future wireless communication applications.

CONFLICT OF INTEREST

The authors declare that they have no potential conflicts of interest related to the work presented in this manuscript.

ACKNOWLEDGMENT

The authors are extremely grateful to the University Grants Commission (UGC), India for providing NET JRF financial assistance to the first author (UGC-Ref. No.: 3770/ (NET-DEC 2018)).

REFERENCES

1. Garg, R., P. Bhartia, I. Bahl, and A. Ittipiboon, *Microstrip Antenna Design Handbook*, Artech House, 2001.
2. Singh, I. and V. S. Tripathi, "Micro strip patch antenna and its applications: A survey," *International Journal of Computer Applications in Technology*, Vol. 2, No. 5, 1595–1599, 2011.
3. Khanna, G. and N. Sharma, "Fractal antenna geometries: A review," *International Journal of Computer Applications*, Vol. 153, No. 7, 29–32, 2016, https://doi.org/10.5120/ijca2016912106.
4. Naqvi, S. A., "Miniaturized triple-band and ultra-wideband (UWB) fractal antennas for UWB applications," *Microwave and Optical Technology Letters*, Vol. 59, No. 7, 1542–1546, 2017, https://doi.org/10.1002/mop.30582.
5. Kordzadeh, A. and F. Hojat-Kashani, "A new reduced size microstrip patch antenna with fractal shaped defects," *Progress In Electromagnetics Research B*, Vol. 11, 29–37, 2009.
6. Ali, J., S. Abdulkareem, A. Hammoodi, A. Salim, M. Yassen, M. Hussan, and H. Al-Rizzo, "Cantor fractal-based printed slot antenna for dual-band wireless applications,"

International Journal of Microwave and Wireless Technologies, Vol. 8, No. 2, 263–270, 2016, https://doi.org/10.1017/S1759078714001469.

7. Chen, W.-L., G.-M. Wang, and C.-X. Zhang, "Small-size microstrip patch antennas combining koch and sierpinski fractal-shapes," *IEEE Antennas and Wireless Propagation Letters*, Vol. 7, 738–741, 2008, https://doi.org/10.1109/LAWP.2008.2002808.
8. Ahmed, Z., A. Muhammad, and M. B. Ihsan, "Improving the sidelobe level, return loss and bandwidth of notch-loaded TM_{30} mode patch via fractal-slot," *IEEE Access*, Vol. 10, 19917–19924, 2022, https://doi.org/10.1109/ACCESS.2022.3152565.
9. Costantine, J., Y. Tawk, S. E. Barbin, and C. G. Christodoulou, "Reconfigurable antennas: Design and applications," *Proceedings of the IEEE*, Vol. 103, No. 3, 424–437, 2015, https://doi.org/10.1109/JPROC.2015.2396000.
10. Chattha, H. T., M. Hanif, X. Yang, Q. H. Abbasi, and I. E. Rana, "Frequency reconfigurable patch antenna for 4G LTE applications," *Progress In Electromagnetics Research M*, Vol. 69, 1–13, 2018.
11. Saroj, A. K. and J. A. Ansari, "A reconfigurable multiband rhombic shaped microstrip antenna for wireless smart applications," *International Journal of RF and Microwave Computer-Aided Engineering*, Vol. 30, No. 10, 2020, https://doi.org/10.1002/mmce.22378.
12. Tripathi, S., A. Mohan, and S. Yadav, "A compact frequency-reconfigurable fractal UWB antenna using reconfigurable ground plane," *Microwave and Optical Technology Letters*, Vol. 59, No. 8, 1800–1808, 2017, https://doi.org/10.1002/mop.30631.
13. Yang, S. S., A. A. Kishk, and K. Lee, "Frequency reconfigurable U-slot microstrip patch antenna," *IEEE Antennas and Wireless Propagation Letters*, Vol. 7, 127–129, 2008, https://doi.org/10.1109/LAWP.2008.921330.
14. Zhang, Y., B.-Z., Wang, X.-S., Yang, and W. Wu, "A fractal Hilbert microstrip antenna with reconfigurable radiation patterns," *2005 IEEE Antennas and Propagation Society International Symposium*, Vol. 3A, 254–257, 2005, https://doi.org/10.1109/APS.2005.1552228.
15. Elwi, T. A., "Remotely controlled reconfigurable antenna for modern 5G networks applications," *Microwave and Optical Technology Letters*, Vol. 63, No. 8, 2018–2023, 2020, https://doi.org/10.1002/mop.32505.
16. Cheng, H.-Y. and J.-S. Row, "A pattern reconfigurable design based on a slotted patch antenna with two feed ports," *Microwave and Optical Technology Letters*, Vol. 63, No. 12, 3035–3040, 2021, https://doi.org/10.1002/mop.33012.
17. Majid, H. A., M. K. A. Rahim, M. R. Hamid, and M. F. Ismail, "Frequency and pattern reconfigurable slot antenna," *IEEE Transactions on Antennas and Propagation*, Vol. 62, No. 10, 5339–5343, 2014, https://doi.org/10.1109/TAP.2014.2342237.
18. Andrenko, A. S., I. V. Ivanchenko, D. I. Ivanchenko, S. Y. Karelin, A. M. Korolev, E. P. Laz'ko, and N. A. Popenko, "Active broad X-band circular patch antenna," *IEEE Antennas and Wireless Propagation Letters*, Vol. 5, 529–533, 2006, https://doi.org/10.1109/LAWP.2005.860200.
19. Singh, A., S. Vijay, and R. N. Baral, "Low cross-polarization improved-gain rectangular patch antenna," *Electronics*, Vol. 8, No. 10, 1189, 2019, https://doi.org/10.3390/electronics8101189.
20. Zhu, Z., C. Chen, Y. Chen, and W. Wu, "A broadband low cross-polarization u-slot patch antenna array based on differential feed," *Progress In Electromagnetics Research C*, Vol. 68, 211–219, 2016.
21. Chen, C., C. Li, Z. Zhu, and W. Wu, "Wideband and low-cross-polarization planar annual ring slot antenna," *IEEE Antennas and Wireless Propagation Letters*, Vol. 16, 3009–3013, 2017, https://doi.org/10.1109/LAWP.2017.2757963.
22. Guo, Y.-X., K.-W. Khoo, L. C. Ong, and K. M. Luk, "Broadband low cross-polarization patch antenna," *Radio Science*, Vol. 42, No. 05, 1–8, 2007, https://doi.org/10.1029/2006RS003595.
23. Ali, T., N. Fatima, and R. C. Biradar, "A miniaturized multiband reconfigurable fractal slot antenna for GPS/GNSS/Bluetooth/WiMAX/X-band applications," *AEU — International Journal of Electronics and Communications*, Vol. 94, 234–243, 2018, https://doi.org/10.1016/j.aeue.2018.07.017.

24. Tirunagari, A., B. Madhav, C. V. Kumar, P. Sruthi, M. Sahithi, and K. V. Manikanta, "Design of a frequency reconfigurable fractal antenna for Internet of Things (IoT) in vehicular communication," *International Journal of Recent Technology and Engineering*, Vol. 7, No. 6, 1605–1611, 2019.
25. K, M. and S. P. Hegde, "Reconfigurable fractal microstrip antenna with varactor diode," *Global Transitions Proceedings*, Vol. 3, No. 1, 183–189, 2022, https://doi.org/10.1016/j.gltp.2022.03.007.
26. Hong, K.-D., X. Chen, X. Zhang, L. Zhu, and T. Yuan, "A slot-loaded high-gain circular patch antenna with reconfigurable orthogonal polarizations and low cross polarization," *IEEE Antennas and Wireless Propagation Letters*, Vol. 21, No. 3, 511–515, 2022, https://doi.org/10.1109/LAWP.2021.3136680.
27. Balanis, C. A., *Antenna Theory, Analysis and Design*, John Wiley and Sons, 2005.
28. Campbell, M., "5.6 scaling and the Hausdorff dimension," *Annennberg Learner: MATHematics Illuminated*, 2013.
29. Duvall, P., J. Keesling, and A. Vince, "The Hausdorff dimension of the boundary of a self-similar tile," *Journal of the London Mathematical Society*, Vol. 61, No. 3, 748–760, 2000, https://doi.org/10.1112/S0024610700008711.
30. https://www.skyworksinc.com/-/media/SkyWorks/Documents/Products/101-200/SMP1340_Series_200051U.pdf.